University of Groningen

Exploring the impact of process parameters on the metal-free light-catalyzed ATRP polymerization of PVDF-based block copolymers

Altomare, Aldo; de Gauw, Vincent; Fiorito, Alice; Loos, Katja

IMPORTANT NOTE: You are advised to consult the publisher's version (publisher's PDF) if you wish to cite from it. Please check the document version below.

Document Version
Publisher's PDF, also known as Version of record

[Link to publication in University of Groningen/UMCG research database](#)
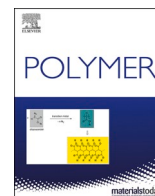
Exploring the impact of process parameters on the metal-free light-catalyzed ATRP polymerization of PVDF-based block copolymers

Aldo Altomare , Vincent de Gauw , Alice Fiorito , Katja Loos [*]

Macromolecular Chemistry and New Polymeric Materials, Zernike Institute for Advanced Materials, University of Groningen, Nijenborgh 4, 9747 AG, Groningen, the Netherlands

ARTICLE INFO

ABSTRACT

The synthesis of well-defined poly(vinylidene fluoride) (PVDF)-based block copolymers has been an important topic in recent years to accurately modify its properties and to achieve high-quality composites. Atom transfer radical polymerization (ATRP) proved itself to be a viable technique for the controlled synthesis of PVDF-based block copolymers. Recently, organic photoredox catalysts (OPRCs) have been reported as effective photocatalysts in light-catalyzed ATRP. Here, we use three OPRs (perylene, 10-methylphenotiazine, 10-phenylphenotiazine) for the ATRP of methylmethacrylate using telechelic PVDF as macroinitiators. We explore the impact of three process parameters: the end group on the polymer chain, the concentration of MMA, and the concentration of the OPRC in solution. First, three different telechelic PVDF were tested under the same monomer and OPRC concentrations to select the best macroinitiator for this system. Then, the effects on the overall control and on the conversion when the concentration of monomer or OPRC is varied were evaluated.

1. Introduction

In recent years, fluoropolymers have attracted wide attention both in industry and academia due to their outstanding thermal, physical and chemical stability [1]. These characteristics depend on the molecular weights, molecular weight distributions, chain configurations, crystalline form, and defects of the polymer chains [2–7]. Polyvinylidene fluoride (PVDF), one of the most important fluoropolymers, is also well known for its piezo-, pyro-, and ferroelectric properties [8–14], especially when it crystallizes in the β crystalline phase, which shows high dielectric permittivity arising from the C–F bonds and the spontaneous orientation of dipoles in the crystalline phase. This makes it attractive for various applications, such as sensors, actuators or dielectric materials for electric storage applications [15–19]. Vinylidene fluoride (VDF) is a gaseous monomer that can be polymerized via radical initiation in a high-pressure vessel. Several studies have been conducted using benzoyl peroxides (BPOs) as initiators for the polymerization of ethylenically unsaturated fluoromonomers [20]. A molecule of modified BPO is homolytically broken into two identical parts, which will independently start a polymerization reaction in the presence of VDF. Two different growing chains will then react with each other through a termination phenomenon that results in chains with half of the peroxide molecule at

each end. A variety of different functional groups can be introduced into BPO by diverse and facile chemistry, and this opens new routes for the synthesis of a variety of block copolymers through different techniques [21,22].

Copolymerization is one of the most powerful tools to modify the properties of PVDF, such as its crystallinity, chemical reactivity, stability, solubility, and processability [23]. Copolymerization is also often necessary to overcome some drawbacks related to the characteristics of PVDF, such as high processing costs or poor solubility in common organic solvents. Moreover, it is also useful to broaden the number of possible applications by increasing its surface energy or the coefficient of friction. Obtaining well-defined copolymers was made possible by the introduction of the controlled/living radical polymerization (CLRP) concept to synthetic polymer chemistry. The outstanding contributions of CLRP, such as atom transfer radical polymerization (ATRP) [24–27], reversible addition-fragmentation chain transfer polymerization or macromolecular design via interchange of xanthates (RAFT/MADIX) [28–30] and iodine transfer polymerization (ITP), have become extremely important for the development of such materials. ATRP, in particular, is a powerful technique that allows well-defined block copolymers with excellent controllability of molecular weight, low dispersity, and high retention of chain end groups to be obtained.
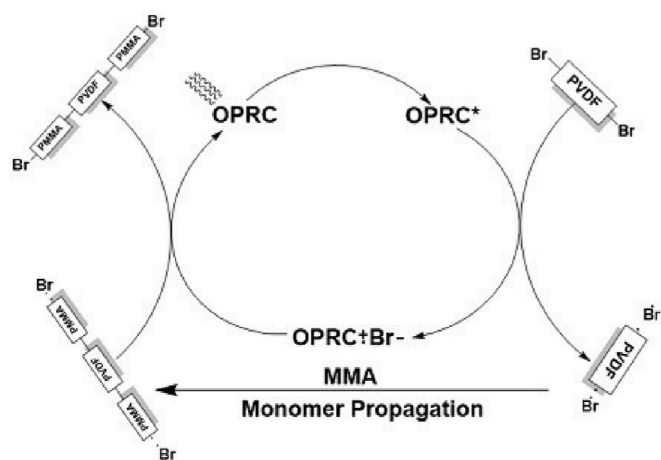

Fig. 1. Mechanism of photoredox-mediated ATRP of bromine-terminated PVDF macroinitiator for the polymerization of MMA under UV–Vis light irradiation with the oxidative quenching pathway.

Generally, it requires a relatively high concentration of a metal catalyst to guarantee control over the whole process and to compensate for the radical termination reactions. For numerous applications, such as biomedicine, biomaterials or microelectronics, metal contamination is a strong limiting factor, despite the elaboration of methods in which the catalyst loading can be reduced below 100 ppm [31–34]. For dielectric materials, it has been shown that even a trace amount of impurity ions can significantly broaden the electric displacement-electric field (D-E) hysteresis loop with consequent high dielectric loss [31,35–37]. The recently developed photoinduced metal-free ATRP [38] has emerged as a powerful methodology to synthesize polymers with the complete elimination of transition metal residues. This synthetic method bears many characteristics of traditional controlled radical polymerization procedures, including good control over molecular weight, low dispersity, and high retention of chain-end functionality. The concept of metal-free ATRP relies on the use of photoredox catalysis, where the excited-state photocatalyst undergoes a reversible electron transfer reaction with an alkyl halide initiator to mediate the exchange between active and dormant species through external light stimulation [39].

Light, as a widely available, relatively safe, and economical external stimulus, has attracted much attention as an initiating factor [40–42] because it can be used with a simple experimental setup under mild reaction conditions, with limited side effects, with the possibility of adjusting the light source and providing spatial and temporal control [41,43–45]. Light of various wavelengths can be effectively used in photocontrolled polymerizations, including UV [40], visible [46,47], and near infrared (NIR) [48,49] light delivered by household bulbs [50], light-emitting diodes (LEDs) [51] or even sunlight [46]. In the past few years, significantly increasing interest has been paid to the development of a variety of low-cost, readily available, and easy-to-use organic photoredox catalysts (OPRCs) for UV and visible light-catalyzed ATRP [39,52–54] that can also be used for the preparation of block copolymers [54–58]. Most photoredox catalysts operate through an oxidative quenching pathway because they possess strongly reducing excited states [E_{red}(PC$^{·+}$/PC*)$\geq$1.5 V vs SCE] that are capable of directly reducing the alkyl bromide or chloride in O-ATRP [52,59], but recently, it has been proven that some OPRC can operate by a reducing quenching pathway by the use of sacrificial electron donors, such as amines, which are oxidized by PC*, generating a more reducing PC radical anion (PC$^{·-}$).

In a paper recently published by our group [59], we tested 5 different organic photoredox catalysts for the synthesis of PVDF-based block copolymers, demonstrating how OPRCs operating through an oxidative quenching pathway (perylene, 10-methylphenotiazine and 10-phenyl-phenotiazine), the mechanism of which is shown in Fig. 1, were able

to effectively control block copolymerization, while OPRCs operating through a reductive quenching pathway (Fig. S1) (fluorescein, eosin Y) were not able to provide good results. Following this study, we decided to investigate this process further, studying the parameters that could influence the metal-free, light-catalyzed process in the synthesis of PVDF-based block copolymers.

Here, we use three different OPRC operating through an oxidative quenching pathway, and we report how varying their concentration in solution, the concentration of the monomer used for the block copolymerization process, or the end-group at the end of the PVDF chain influence the metal-free, light-catalyzed process.

2. Experimental section

2.1. Materials

Methyl methacrylate (MMA, 99%, Sigma Aldrich) was passed through an alumina column to remove the inhibitor, 4-(bromomethyl) benzoic acid (Sigma Aldrich), 4-(1-bromoethyl)benzoic acid (Sigma Aldrich), 4-benzoylbenzoic acid (Sigma Aldrich), oxalyl chloride (99%, Sigma Aldrich), lithium peroxide (Li$_2$O$_2$, 95% Alfa Aesar), sodium borohydride (NaBH$_4$, 99%, Sigma Aldrich), phosphorus tribromide (PBr$_3$, 99%, Sigma Aldrich), magnesium sulfate (MgSO$_4$, 99,5%, Sigma Aldrich), vinylidene fluoride (VDF, 98%, Synquest Lab), 10-methylphe-notiazine (10-MPT, Alfa Aesar), 10-phenylphenotiazine (10-PPT, Sigma Aldrich), perylene (98%, Sigma Aldrich), dichloromethane (DCM, extra dry, 99.8%, Acros Organics), N,N-dimethylformamide (DMF, Anhydrous 99.8%, Thermo Fischer Scientific), n-hexane (99%, Macron Fine Chemicals), diethyl ether (Et$_2$O, Macron Fine Chemicals), chloroform (Macron Fine Chemicals), acetonitrile (99,9+%, extra dry, Acros Organics), methanol (MeOH, Macron Fine Chemicals), ethanol (EtOH, Macron Fine Chemicals), hydrochloric acid (HCl, 37%, Sigma Aldrich) were used as received. LED stripes (395 nm, intensity = 4 W) were purchased from Waveform Lightning, and the TLC lamp (302 nm, intensity = 8 W) was purchased from Thermo Fischer.

2.2. Synthesis of 4-(1-bromomethyl) benzoyl peroxide (MBrBPO)

In a typical reaction, 4-(1-bromomethyl) benzoic acid (3.0 g, 13.9 mmol) was dissolved in 50 mL of anhydrous DCM at 0 °C. Oxalyl chloride (1.5 eq., 20.9 mmol, 1.79 mL) and a few drops of anhydrous DMF were added, and the reaction started. After reacting for 2 h at room temperature, the solvent was removed by rotary evaporation. The remaining yellow residue was immediately dissolved in 100 mL n-hexane/Et$_2$O (1/1). The resulting solution was slowly added via a droplet funnel to a rapidly stirred 50 mL aqueous solution of Li$_2$O$_2$ (1.3 eq, 18.1 mmol, 0.83 g) at 0 °C. After reacting for 2 h at room temperature, the reaction mixture was diluted with 250 mL of chloroform and washed twice with 100 mL of H$_2$O. The aqueous phase was extracted twice with 50 mL of chloroform. The combined organic phases were dried over MgSO$_4$, and chloroform was subsequently removed by rotary evaporation. The remaining yellow solid was recrystallized from chloroform, yielding white needle-shaped crystals.

[1]*H-NMR (400 MHz, DMSO-d$_6$): 8,03 (m, -ArH), 7,55 (m, -ArH), 4,52 (m, -CH$_2$Br).*

2.3. Synthesis of 4-(1-bromoethyl) benzoyl peroxide (EtBrBPO)

In a typical reaction, 4-(1-bromoethyl) benzoic acid (3.0 g, 13.1 mmol) was dissolved in 50 mL of anhydrous DCM at 0 °C. Oxalyl chloride (1.5 eq., 19.6 mmol, 1.7 mL) and a few drops of anhydrous DMF were added, and the reaction started. After reacting for 2 h at room temperature, the solvent was removed by rotary evaporation. The remaining yellow residue was immediately dissolved in 100 mL n-hexane/Et$_2$O (1/1). The resulting solution was slowly added via a droplet funnel to a rapidly stirred 50 mL aqueous solution of Li$_2$O$_2$ (1.3eq, 17.0

mmol, 0.8 g) at 0 °C. After reacting for 2 h at room temperature, the reaction mixture was diluted with 250 mL of chloroform and washed twice with 100 mL of H$_2$O. The aqueous phase was extracted twice with 50 mL of chloroform. The combined organic phases were dried over MgSO$_4$, and chloroform was subsequently removed by rotary evaporation. The remaining yellow solid was recrystallized from chloroform, yielding white needle-shaped crystals.

^{1}H-NMR (400 MHz, DMSO-d_6:8,05 (m, -ArH) 7,58 (m, -ArH), 5,20 (m, -CH(CH$_3$)Br), 2,06 (d, -CH$_3$).

2.4. Synthesis of 4-(bromo(phenyl)methyl) benzoic peroxide (BBrBPO)

In a typical procedure, 4-benzoylbenzoic acid (5.0 g, 22.1 mmol) was dissolved in 20 mL of EtOH. At 0 °C, sodium borohydride (1.5 eq.(1.25 g, 33.1 mol) was added, and the reaction proceeded for 1 h. The reaction was then quenched by adding hydrochloric acid until a pH of approximately 1 was reached. The solvent was then evaporated, giving 4-(hydroxy(phenyl)methyl) benzoic acid. The isolated product (5.0 g, 21.9 mmol) was dissolved in 20 mL of anhydrous DCM, and PBr$_3$ (1.3 eq., 2.7 mL, 24.4 mmol) was added dropwise at 0 °C. The reaction proceeded at room temperature for 3 h and was then quenched by the addition of a few drops of water. The solution was then washed once with 10 mL of brine and twice with 20 mL of water. The organic phase was then dried and evaporated through rotary evaporation, giving 4-(bromo(phenyl) methyl)benzoic acid as a white solid with a yield higher than 80%. The product obtained from the previous step was then reacted with oxalyl chloride (1.5 eq, 2.8 mL, 32.8 mmol) and a few drops of anhydrous DMF in 40 mL of anhydrous DCM at 0 °C. After reacting for 2 h at room temperature, the solvent was removed by rotary evaporation. The remaining white/yellow residue was immediately dissolved in 100 mL of n-hexane:Et$_2$O (1:1). The resulting solution was slowly added via a droplet funnel to a rapidly stirred 50 mL aqueous solution of Li$_2$O$_2$ (1.3 eq, 1.3 g, 28.47 mmol) at 0 °C. After reacting for 3 h at room temperature, the reaction mixture was diluted with 100 mL of chloroform and washed once with 30 mL of brine and twice with 30 mL of H$_2$O. The aqueous phase was extracted twice with 30 mL of chloroform. The combined organic phases were dried over Mg$_2$SO$_4$, and chloroform was subsequently removed by rotary evaporation. The remaining white solid was recrystallized from chloroform and methanol to yield 4-(bromo (phenyl)methyl) benzoic peroxide.

^{1}H-NMR (400 MHz, DMSO-d_6): 8.04 (m, -ArH), 7,77 (m, -ArH), 7,52 (m, -ArH), 7,39 (m, -ArH), 6,78 (s, -CH).

2.5. Synthesis of bromine-terminated PVDF

A typical procedure for the homopolymerization of vinylidene fluoride is as follows: The selected BPO (0.2 mmol) was dissolved in 300 mL of anhydrous acetonitrile, and this solution was charged into a pressure reactor. The vessel was closed and purged with nitrogen for 30 min to degas the mixture. Subsequently, the reactor was charged with 20 bars of VDF, heated to 90 °C, and stirred at 500 rpm. After reacting for 4 h, the vessel was cooled down and depressurized. The solvent was evaporated through rotary evaporation, and the obtained solid was redissolved in DMF. The solution was precipitated in a solution of H$_2$O/MeOH (1/1), washed several times with chloroform, and dried in a vacuum at 50 °C.

MBrPVDF ^{1}H NMR spectrum of 4-(bromomethyl)-terminated PVDF (MBrPVDF).

^{1}H NMR (400 MHz, DMSO-d_6): PVDF head-to-tail (2,89 ppm) and PVDF tail-to-tail (2,25 ppm), 7,77 ppm (m, -ArH), 6,80 ppm (m, -ArH), 4,77 ppm (m, -CH$_2$Br).

EtBrPVDF ^{1}H NMR spectrum of 4-(bromoethyl)-terminated PVDF (EtBrPVDF).

^{1}H NMR (400 MHz, DMSO-d_6): PVDF head-to-tail (2.89 ppm) and PVDF tail-to-tail (2,25 ppm), 8,00 ppm (m, -ArH), 7,69 ppm (m, -ArH), 4,23 ppm (m,-CH(CH$_3$)Br), 2,00 ppm (d, -CH$_3$).

BBrPVDF ^{1}H NMR spectrum of 4-(bromo(phenyl)ethyl)-terminated PVDF (BBrPVDF).

^{1}H NMR (400 MHz, DMSO-d_6): PVDF head-to-tail (2.89 ppm) and PVDF tail-to-tail (2,25 ppm), 8.50 ppm (m, -ArH), 8,15 ppm (m, -ArH), 7,99 ppm (m, -ArH), 7,82 ppm (m, -ArH), 7,06 ppm (s, -CH).

2.6. Synthesis of PMMA-b-PVDF-b-PMMA through an oxidative quenching pathway

A typical procedure for the ATRP of PMMA through an oxidative quenching pathway is as follows: A Schlenk quartz tube was dried using a heat gun and filled with nitrogen. Two milliliters of DMF was added together with 0.3 g of the selected bromine-terminated PVDF and the desired amount of the selected OPRC (perylene, 10-PPT or 10- MPT). The desired amount of MMA was added through a degassed syringe, and the reaction mixture was degassed for 30 min using nitrogen. The reaction started when the light of the wavelength corresponding to the OPRC used was turned on and proceeded for the desired amount of time. The reaction mixture was then precipitated in a solution of H$_2$O/MeOH (1/1) (20x the volume of the reaction mixture). The obtained white powder was soaked in chloroform under vigorous stirring to dissolve the homopolymer PMMA formed as a byproduct of the reaction. The triblock copolymer PMMA-*b*-PVDF-*b*-PMMA was not dissolved by chloroform and was recovered through centrifugation. The soaking-centrifugation process was repeated several times until the integral of the ^{1}H NMR peaks related to the PMMA block remained stable. ^{1}H NMR spectrum of PMMA-b-PVDF-b-PMMA.

^{1}H NMR (400 MHz, DMSO-d_6): 2,94 ppm (t, -CF$_2$CH$_2$-CF$_2$CH$_2$-, head-to-tail), 2,35 ppm (t, -CF$_2$CH$_2$–CH$_2$CF$_2$-, tail-to-tail), 3,63 ppm (s,-OCH$_3$), 0,9-1,0 ppm (-CH$_2$-C(CH$_3$)-).

2.7. Kinetic studies

The kinetics of the reactions were followed by both monomer consumption and block copolymerization. The monomer consumption was followed directly from the reaction mixture. At selected intervals of time, one drop of the reaction mixture was withdrawn and directly dissolved in DMSO-d_6. The DMF peak at 7.9 ppm was used as an internal reference, and the ratio between the integral of the peaks related to the double bond (6.0 ppm and 5.7 ppm) of the monomer, which is consumed during the reaction, at t_0 and the same peaks at t_x were used to study the kinetics of monomer consumption. The block copolymerization was followed by withdrawing 0.2 mL of the reaction mixture and precipitating it in 4 mL of a solution of H$_2$O/MeOH (1/1). To remove the PMMA homopolymer formed during the process, the product was soaked in chloroform under vigorous stirring. Chloroform selectively dissolves the PMMA homopolymer and does not dissolve the triblock copolymer PMMA-*b*- PVDF-*b*-PMMA. The product of interest was separated from chloroform through centrifugation and dried in a vacuum oven at 50 °C before being analyzed through ^{1}H NMR. The soaking-centrifuge process was repeated several times until the integral of the ^{1}H NMR peaks related to the PMMA block remained stable. The conversion was calculated using the PVDF peaks at 2.94 ppm and 2.35 ppm as internal standards and following the increase in the area of the peak related to the -OCH$_3$ group on the PMMA block (3.6 ppm). The conversion was calculated using (1):

$$Conversion\ (\%) = \frac{2}{3} * \frac{I(PMMA)}{I(PVDF) + I(PVDF)} * 100 \qquad (1)$$

The conversion calculated with eq (1), often also referred to as "initiation efficiency" is calculated using the PVDF block as the standard and following the growth of the PMMA blocks on the macroinitiator.

3. Results and discussion

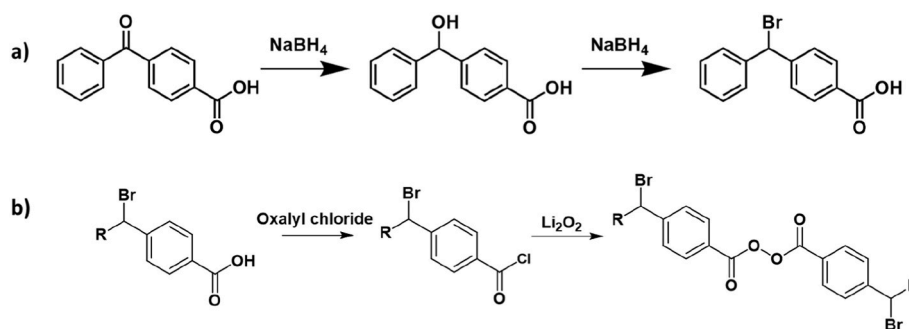To investigate the effect of different end groups on the PVDF chains

Fig. 2. (a) Synthetic pathway for the synthesis of 4-(bromo(phenyl)methyl)benzoic acid. (b) Synthetic pathway for the synthesis of functionalized BPOs. R=H, CH3, Benzene.
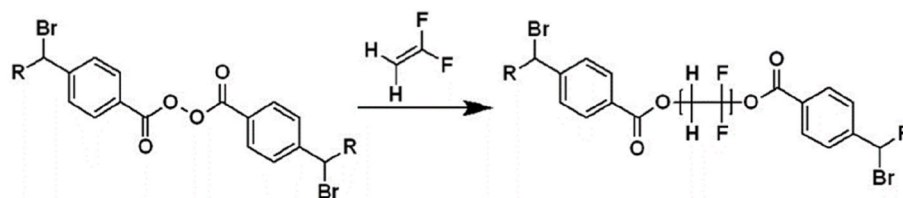

Fig. 3. Reaction scheme of the homopolymerization of VDF using a functionalized BPO as a radical provider. R=H, CH$_3$, benzene.

during the block copolymerization process, three modified BPOs (4-(bromomethyl)benzoyl peroxide, 4-(1-bromoethyl)benzoyl peroxide, and 4-(bromo(phenyl)methyl)-benzoyl peroxide) were synthesized and used for the homopolymerization of VDF. The resulting telechelic PVDF with the selected end groups can be used as initiators in the subsequent ATRP process. These BPOs were chosen due to their facile synthesis and the presence of a C–Br bond that can be used in the subsequent ATRP process. The stability of the radicals formed when the C–Br bond is broken differs among these three BPOs. The predicted order of stability was 4-(bromo(phenyl)methyl)benzoyl peroxide > 4-(1-bromoethyl) benzoyl peroxide > 4-(bromomethyl) benzoyl peroxide [60].

4-(Bromomethyl) benzoyl peroxide and 4-(1-bromoethyl)benzoyl peroxide were easily synthesized from the corresponding benzoic acid through the two-step reaction shown in Fig. 2b, while the synthetic pathway toward 4-(bromo(phenyl)methyl)benzoyl peroxide required more steps, rendering its synthesis slightly more complicated and more prone to impurities in the final product (Fig. 2a).

The ^{1}H NMR analysis (Figs. S2–S4) showed that all three functional benzoyl peroxides were successfully synthesized, as all peaks related to the protons of the three different products (assigned in the experimental section) were clearly visible.

Functionalized benzoyl peroxides have been demonstrated to act as efficient initiators for the preparation of PVDF and other fluoropolymers [61,62], so all three previously synthesized BPOs were used for the homopolymerization of VDF to obtain a macroinitiator with ATRP-active end groups.

Telechelic PVDF was successfully synthesized via the synthetic procedure shown in Fig. 3, as confirmed by ^{1}H NMR analysis (assigned in the experimental section and Figs. S4–S10).

The absence of termination through disproportionation [20,63] is confirmed by the absence of resonances due to unsaturated bonds. Reaction times were limited to 4 h to minimize chain transfer reactions that can occur in the system. Traces of -CH$_2$-CF$_2$H (6.3 ppm) and -CF$_2$-CH$_3$ (1.8 ppm) moieties were attributed to intramolecular backbiting that resulted in short chain branches (Figs. S4–S10). The macroinitiators were characterized through GPC and showed the characteristic negative peak obtained for fluorinated polymers (Fig. S11). We obtained an M$_w$ of approximately 14000 D in all cases with a dispersity of approximately 1.5, which is quite common for polymers synthesized through free

Table 1
Monomer consumed and conversion obtained for the three selected macroinitiators with each of the OPRC.

OPRC	Functional Group	Monomer Consumed (%)	Conversion (%)
Perylene	MBr	44	13
Perylene	EtBr	42	43
Perylene	BBr	59	27
10-PPT	MBr	70	23
10-PPT	EtBr	53	26
10-PPT	BBr	59	13
10-MPT	MBr	49	15
10-MPT	EtBr	63	36
10-MPT	BBr	46	10

radical polymerization initiated by benzoyl peroxides. These polymers were all used as macroinitiators for the metal-free light-catalyzed ATRP of MMA for the synthesis of PVDF-based block copolymers (Figs. S12–S13).

3.1. Effect of the functional group on the macroinitiator

Starting from the results obtained in our previous work [59], we used the three different macroinitiators described in the previous section as starting materials for the synthesis of PVDF-based block copolymers using methyl methacrylate as the monomer for the new blocks and perylene, 10-methylphenotiazine and 10-phenylphenotiazine, irradiated with light of suitable wavelength (Figs. S14–S18), as organic photoredox catalysts. The ratio between the macroinitiator and the OPRC and between the macroinitiator and the monomer was kept the same in all cases ([RPVDF]:[OPRC] = [1]:[0.25], [RPVDF]:[MMA] = [1]:[180]; R = methyl-bromide (MBr), ethyl-bromide (EtBr), benzoyl-bromide (BBr)), while the type of macroinitiator was varied. The results are summarized in Table 1 and are depicted in Fig. 4a and 4b.

Fig. 4a shows that the consumption of monomer is linear over time, regardless of the OPRC used and the functional group of the PVDF main chain. The conversion (Fig. 4b) is more affected by the choice of end group. In all cases, higher values of conversion are reached when the macroinitiator bearing the ethyl-bromide end group is used. It is not
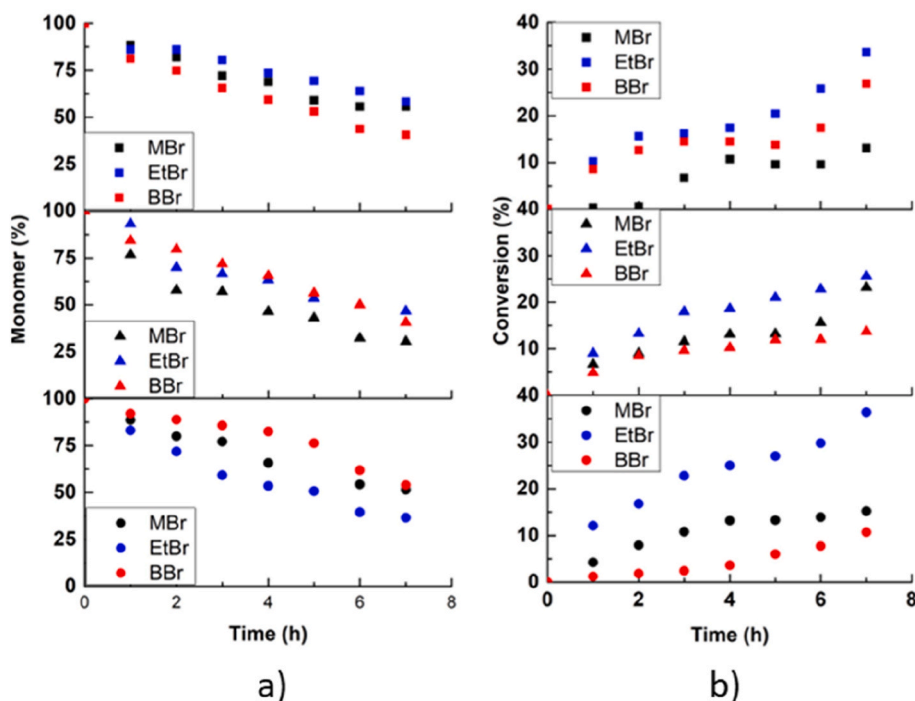
Fig. 4. a) Kinetics of the consumption of MMA during the block copolymerization reaction using MBrPVDF (black), EtBrPVDF (blue), and BBrPVDF (red) as macroinitiators and perylene (square), 10-PPT (triangle), and 10-MPT (circle) as OPRC. b) Kinetics of the conversion of MMA during the block copolymerization reaction using MBrPVDF (black), EtBRPVDF (blue), and BBrPVDF (red) as macroinitiators and perylene (square), 10-PPT (triangle), and 10-MPT (circle) as the OPRC. (For interpretation of the references to colour in this figure legend, the reader is referred to the Web version of this article.)
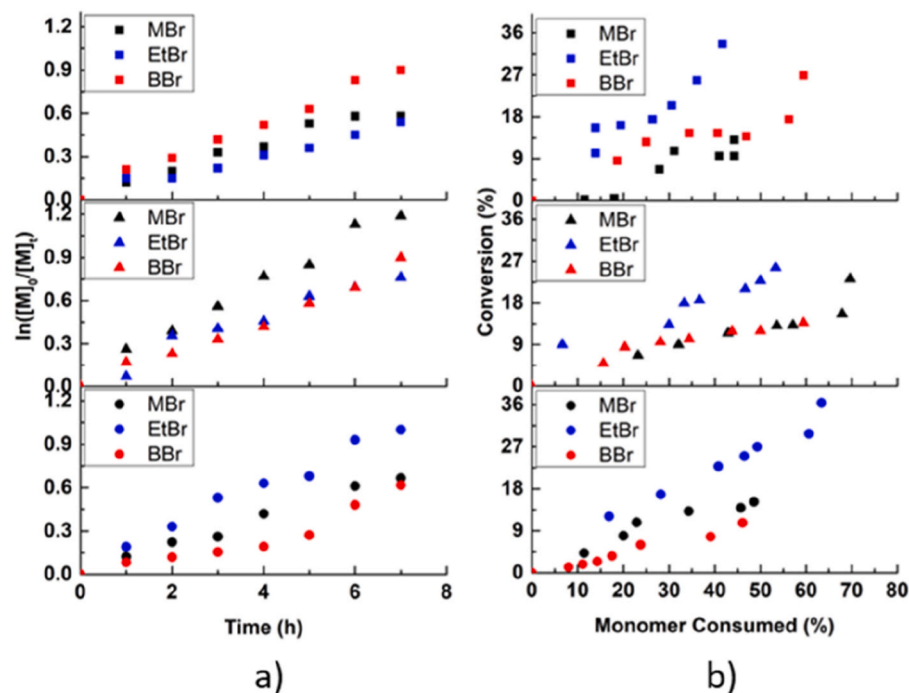

Fig. 5. a) Semilogarithmic plot of the monomer consumption during the block copolymerization of MMA with MBrPVDF (black), EtBrPVDF (blue), BBrPVDF (red) as macroinitiators and perylene (square), 10-PPT (triangle), 10-MPT (circle) as OPRC. b) Plot of the conversion (%) vs the monomer consumption (%) for the block copolymerization of MMA with MBrPVDF (black), EtBrPVDF (blue), BBrPVDF (red) as macroinitiators and perylene (square), 10-PPT (triangle), 10-MPT (circle) as OPRC. (For interpretation of the references to colour in this figure legend, the reader is referred to the Web version of this article.)

surprising that worse results are obtained when the macroinitiator bearing the methyl-bromide end group is used, since the stability of the formed radical is lower than in the case of EtBrPVDF. It is more surprising that the macroinitiator with a benzoyl-bromide end group also produces worse results. This may be due to the longer synthesis procedure for this initiator, which results in byproducts that are difficult to separate from the desired product and can negatively impact the purity of the synthesized macroinitiator, as seen in the ^{1}H NMR spectrum for this end-group (Fig. S10).

The semilogarithmic plot of the monomer consumption versus time,

seen in Fig. 5a, shows first-order kinetics in all cases. When the monomer consumed (%) is plotted against the conversion (%) (Fig. 5b), a linear relationship is observed when EtBrPVDF is used with all three OPRCs, indicating a controlled process. When the macroinitiator with the benzoyl-bromide end group is used, a linear relationship is observed when 10-PPT and 10-MPT are used, but the curve does not appear to follow a linear trend when perylene is used. Nonperfect linearity is also observed when MBrPVDF is used, indicating that a less stable radical leads to less control over the polymerization. Based on these results, we decided to use EtBrPVDF for the next two parts of this study.

Table 2
Monomer consumed and conversion obtained when changing the concentration of the monomer for each of the selected OPRC.

OPRC	[MMA]	Monomer Consumed (%)	Conversion (%)
Perylene	[90]	41	12
Perylene	[180]	42	34
Perylene	[360]	49	64
10-PPT	[90]	64	5
10-PPT	[180]	53	26
10-PPT	[360]	73	36
10-MPT	[90]	74	17
10-MPT	[180]	63	36
10-MPT	[360]	64	47

3.2. Effect of different MMA/PVDF ratios

The effect of the monomer concentration on the block copolymerization of PVDF-based block copolymers was studied. The functional group on the macroinitiator was kept the same (EtBrPVDF), and the concentration of the OPRC was kept constant at a ratio of [1]:[0.25] in relation to the macroinitiator. The concentration of the monomer was varied to [EtBrPVDF]:[MMA] = [1]:[90], [1]:[180], and [1]:[360]. The results are summarized in Table 2.

Fig. 6a clearly shows that the monomer is consumed linearly in all cases with time, except for the case in which 10-PPT is used with a ratio [EtBrPVDF]:[MMA] = [1]:[90]. A similar percentage of monomers is consumed in all cases when perylene and 10-MPT are used, while a larger variation is seen when 10-PPT is used. The concentration of monomer significantly impacts the conversion achieved (Fig. 6b). In all cases, the conversion increases with an increase in the monomer concentration. When perylene is used as an OPRC, increasing the monomer concentration from a ratio of [1]:[90] between the macroinitiator and the monomer to [1]:[360] results in a conversion increase from approximately 10% to almost 60%. When 10-PPT is used, the conversion follows the same trend but only reaches approximately half the conversion values achieved with perylene. Similarly, when 10-MPT is used, the trend remains the same, but 10-MPT and perylene reach similar conversion values at a ratio of [1]:[180] between EtBrPVDF and MMA. However, decreasing the concentration of monomer leads to better conversion values with 10-MPT, while increasing the amount of monomer leads to much higher conversion values with perylene. This is likely due to the lower wavelength used with 10-MPT, which more easily triggers the homopolymerization of MMA and makes the reaction mixture more viscous, slowing down the block copolymerization process while consuming the available monomer more quickly as a byproduct.

Fig. 7a shows first-order kinetics in all cases, especially when perylene and 10-MPT are used. A nonperfect trend is visible in the case of 10-PPT when the concentration of the monomer is reduced. These results are confirmed by the plots of conversion vs monomer consumed (Fig. 7b), in which good linearity is seen in all cases - a sign that the process occurs in a controlled fashion. These first results confirm that the three photoredox catalysts offer good control over the ATRP process using PVDF as a macroinitiator, even when the concentration of monomer is changed. Changing the concentration of monomers influences the conversion, which follows a common trend in all cases: the conversion increases when the monomer concentration is increased, but this does not influence the properties of the studied process, which remained controlled.

3.3. Effect of the OPRC/PVDF ratio

The last studied parameter was the effect of the concentration of the photoredox catalyst used. The functional group on the macroinitiator used was kept the same (EtBrPVDF), and the concentration of the monomer was kept constant to a ratio [1]:[180] with the macroinitiator, while the concentration of the OPRC was varied to be [EtBrPVDF]:[OPRC] = [1]:[2.5], [1]:[0.25], and [1]:[0.025]. The results obtained are summarized in Table 3.

Fig. 8a and 8b show how in all cases, increasing the concentration of OPRC to [1]:[2.5] leads to lower consumption of monomer and therefore leads to a lower conversion in every case. When perylene is used, a similar percentage of monomer is consumed when the ratio is [EtBrPVDF]:[OPRC] = [1]:[0.25] or lowered to [EtBrPVDF]:[OPRC] = [1]:[0.025], and a similar result is obtained in the case of 10-PPT.

When 10-MPT is used, a higher percentage of monomer is consumed when the ratio is [1]:[0.25] compared to when the ratio is [1]:[0.025]. When perylene is used, a huge effect of the OPRC concentration is visible on the conversion, which increases by lowering the concentration of the
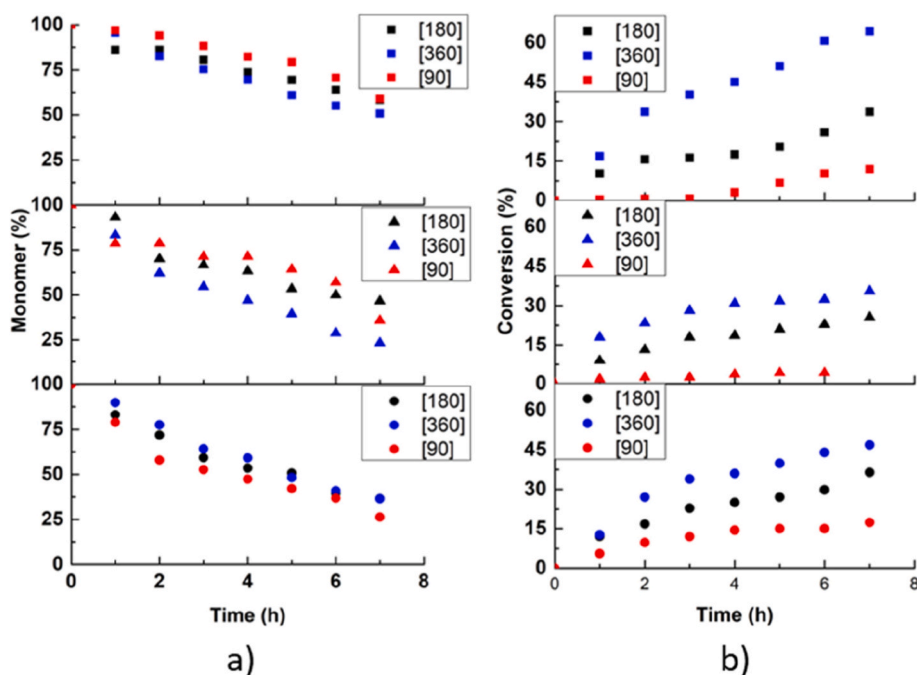

Fig. 6. a) Kinetics of the consumption of MMA during the block copolymerization reaction using the ratio between the macroinitiator and monomer: [EtBrPVDF]:[MMA] = [1]:[90] (red), [1]:[180] (black), [1]:[360] (blue), and perylene (square), 10-PPT (triangle), 10-MPT (circle) as OPRC. b) Kinetics of the conversion of MMA during the block copolymerization reaction using the ratio between the macroinitiator and monomer: [EtBrPVDF]:[MMA] = [1]:[90] (red), [1]:[180] (black), [1]:[360] (blue), and perylene (square), 10-PPT (triangle), 10-MPT (circle) as OPRC. (For interpretation of the references to colour in this figure legend, the reader is referred to the Web version of this article.)

Fig. 7. a) Semilogarithmic plot of the monomer consumption during the block copolymerization of MMA with EtBrPVDF using the ratio between the macroinitiator and monomer: [EtBrPVDF]:[MMA] = [1]:[90] (red), [1]:[180] (black), [1]:[360] (blue), and perylene (square), 10-PPT (triangle), 10-MPT (circle) as OPRC. b) Plot of the conversion (%) vs the monomer consumption (%) for the block copolymerization of MMA with EtBrPVDF using the ratio between the macroinitiator and monomer: [EtBrPVDF]:[MMA] = [1]:[90] (red), [1]:[180] (black), [1]:[360] (blue), and perylene (square), 10-PPT (triangle), 10-MPT (circle) as OPRC. (For interpretation of the references to colour in this figure legend, the reader is referred to the Web version of this article.)
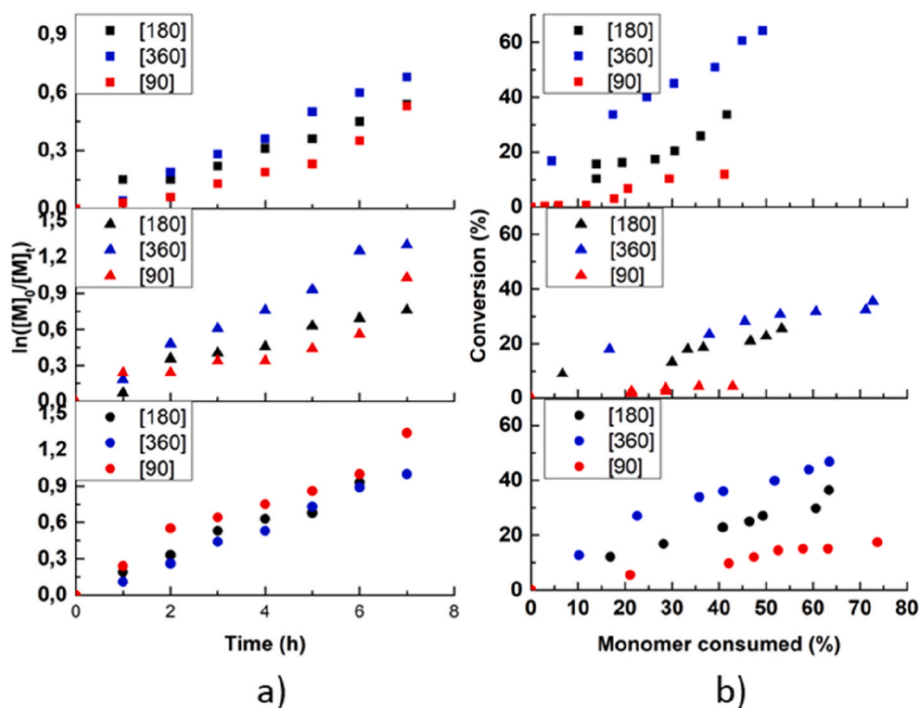
Table 3
Monomer consumed and conversion obtained when changing the concentration of the monomer for each of the selected OPRC.

OPRC	[OPRC]	Monomer Consumed (%)	Conversion (%)
Perylene	[2.5]	27	10
Perylene	[0.25]	42	34
Perylene	[0.025]	49	51
10-PPT	[2.5]	41	10
10-PPT	[0.25]	53	26
10-PPT	[0.025]	54	26
10-MPT	[2.5]	37	25
10-MPT	[0.25]	63	36
10-MPT	[0.025]	49	33

OPRC, but without losing its linearity over time. When 10-PPT and 10-MPT are used, the conversion reaches lower values when the ratio is set at [1]:[2.5]. Decreasing the concentration from [1]:[0.25] to [1]:[0.025] does not have any influence on the conversion, which reaches similar values in both cases. In the case of 10-PPT and 10-MPT, decreasing the amount of OPRC does not influence the overall process, while in the case of perylene, lowering the amount of OPRC gives higher values of conversion. In all cases, increasing the amount of OPRC gives worse results in terms of conversion.

From Fig. 9a, it is possible to see, once again, first-order kinetics indicating a constant concentration of radicals over time. A certain linearity is seen when the conversion is plotted against the percentage of monomer consumed (Fig. 9b). This proves how varying the concentration of the OPRC does not negatively affect the control over the polymerization. These data show how increasing the concentration of the OPRC to [1]:[2.5] slows down the monomer consumed and decreases the conversion reached. In the case of perylene, decreasing the amount of OPRC results in an increase in the values of conversion reached, while it does not influence the values of conversion reached when 10-PPT or 10-MPT are used. Table S1 in Supporting Info, shows the Mw and composition of all the synthesized block copolymers at time 7 h (time of the last kinetic point taken) in the different conditions reported in this paper.

4. Conclusions

In conclusion, our study delves into the intricacies of metal-free light-catalyzed atom transfer radical polymerization for the synthesis of PVDF-based block copolymers. Three organic photoredox catalysts, operating through an oxidative quenching pathway, were tested, uncovering the effect of various parameters on the process. Our findings highlight the superiority of using ethyl-bromide terminated PVDF as the macroinitiator, as it provides optimal results in terms of conversion and control.

This research shows that adjusting the concentration of the monomer and organic photoredox catalyst can be leveraged to achieve the desired final conversion. Increasing the monomer concentration leads to a higher conversion, while decreasing the concentration of the OPRC results in higher conversions with equal monomer amounts, without negatively impacting the control over the process.

These findings open up new avenues for tuning the process to achieve the desired properties in the final material. Whether it is a high or low conversion that is desired, the amount of monomer and OPRC can be adjusted accordingly.

This paves the way for creating well defined PVDF-based block copolymers, scaling up the reagents depending on the final properties desired. This metal-free synthesis enables PVDF-based block copolymers to be used in new and exciting applications such as biomedical, microelectronics, or all of those applications in which metal contamination is a huge drawback.

CRediT authorship contribution statement

Aldo Altomare: Conceptualization, Methodology, Formal analysis, Validation, Writing – original draft, Supervision. **Vincent de Gauw:** Formal analysis, Investigation, Writing – review & editing. **Alice Fiorito:** Formal analysis, Investigation, Writing – review & editing. **Katja Loos:** Resources, Writing – review & editing, Supervision, Funding acquisition.
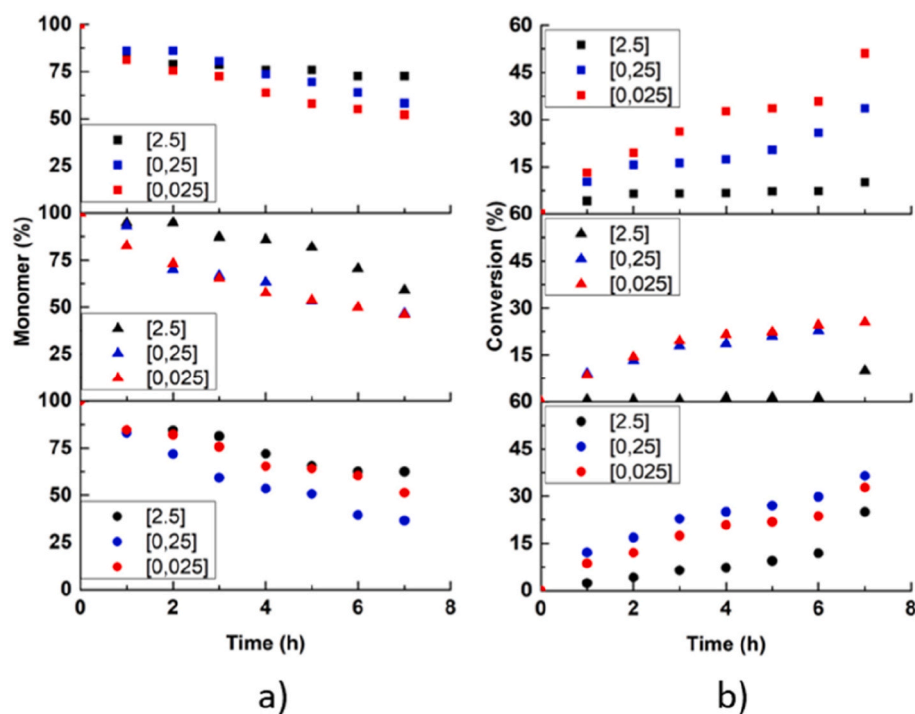
Fig. 8. a) Kinetics of the consumption of MMA during the block copolymerization reaction using the ratio between the macroinitiator and the organic photo-redox catalyst: [EtBrPVDF]:[OPRC] = [1]:[2.5] (black), [1]:[0.25] (blue), [1]:[0.025] (red), and perylene (square), 10-PPT (triangle), 10-MPT (circle) as OPRC. b) Kinetics of the conversion of MMA during the block copolymerization reaction using the ratio between the macroinitiator and the organic photo-redox catalyst: [EtBrPVDF]:[OPRC] = [1]:[2.5] (black), [1]:[0.25] (blue), [1]:[0.025] (red), and perylene (square), 10-PPT (triangle), 10-MPT (circle) as OPRC. (For interpretation of the references to colour in this figure legend, the reader is referred to the Web version of this article.)

Fig. 9. a) Semilogarithmic plot of the monomer consumption during the block copolymerization of MMA with EtBrPVDF using the ratio between the macroinitiator and the organic photoredox catalyst: [EtBrPVDF]:[OPRC] = [1]:[2.5] (black), [1]:[0.25] (blue), [1]:[0.025] (red), and perylene (square), 10-PPT (triangle), 10-MPT (circle) as OPRC. b) Plot of the conversion (%) vs the monomer consumption (%) for the block copolymerization of MMA with EtBrPVDF using the ratio between the macroinitiator and the organic photoredox catalyst: [EtBrPVDF]:[OPRC] = [1]:[2.5] (black), [1]:[0.25] (blue), [1]:[0.025] (red), and perylene (square), 10-PPT (triangle), 10-MPT (circle) as OPRC. (For interpretation of the references to colour in this figure legend, the reader is referred to the Web version of this article.)
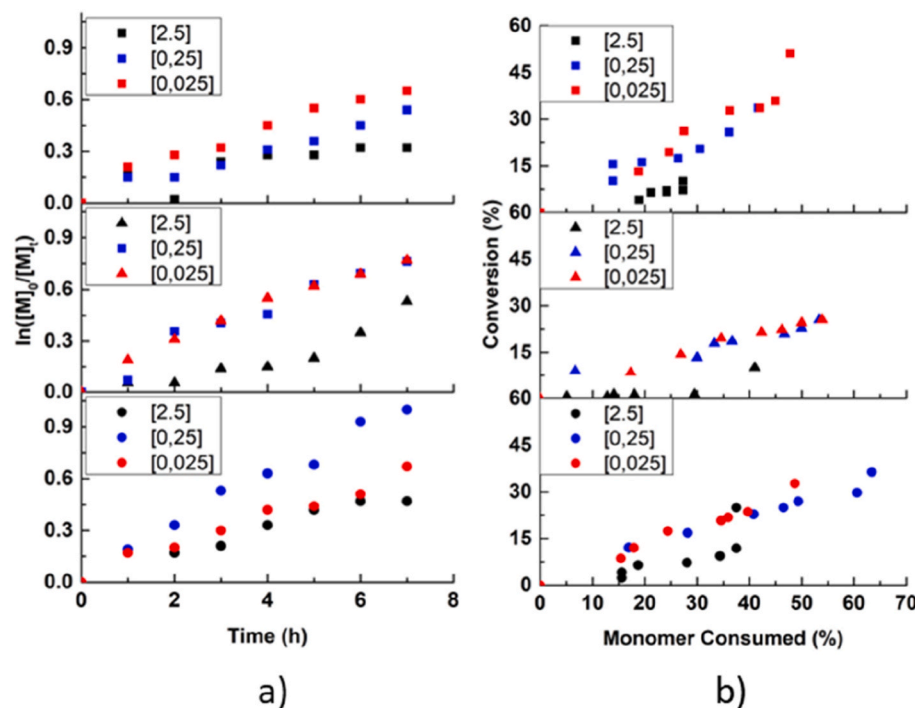
Declaration of competing interest

The authors declare that they have no known competing financial interests or personal relationships that could have appeared to influence the work reported in this paper.

Data availability

Data will be made available on request.

Appendix A. Supplementary data

Supplementary data to this article can be found online at https://doi.org/10.1016/j.polymer.2023.126145.

References

[1] B. Ameduri, B. Boutevin, G. Kostov, Fluoroelastomers: synthesis, properties and applications, Prog. Polym. Sci. 26 (2001) 105–187.

[2] B. Ameduri, Copolymers of vinylidene fluoride with functional comonomers and applications therefrom: recent developments, challenges and future trends, Prog. Polym. Sci. 133 (2022), 101591.

[3] A. Taguet, B. Ameduri, B. Boutevin, Crosslinking of vinylidene fluoride-containing fluoropolymers, Crosslinking in Materials Science (2005) 127–211.

[4] S. Ebnesajjad, Introduction to Vinylidene Fluoride Polymers, Introduction to Fluoropolymers, 2013, pp. 133–148.

[5] J.G. Drobny, Technology of Fluoropolymers, 2008.

[6] F.A. Bovey, Chain Structure and Conformation of Macromolecules, Academic Press, 1982.

[7] B. Ameduri, From vinylidene fluoride (VDF) to the applications of VDF-containing polymers and copolymers: recent developments and future trends, Chem. Rev. 109 (12) (2009) 6632–6686.

[8] V.V. Kochervinskii, The properties and applications of fluorine-containing polymer films with piezo- and pyro-activity, Russ. Chem. Rev. 63 (4) (1994) 367.

[9] H. Xu, Z.Y. Cheng, D. Olson, T. Mai, Q.M. Zhang, G. Kavarnos, Ferroelectric and electromechanical properties of poly (vinylidene-fluoride–trifluoroethylene–chlorotrifluoroethylene) terpolymer, Appl. Phys. Lett. 78 (16) (2001) 2360–2362.

[10] Z.Y. Cheng, V. Bharti, T.B. Xu, S. Wang, Q.M. Zhang, T. Ramotowski, F. Tito, R. Ting, Transverse strain responses in electrostrictive poly (vinylidene fluoride-trifluoroethylene) films and development of a dilatometer for the measurement, J. Appl. Phys. 86 (4) (1999) 2208–2214.

[11] M. Wegener, W. Kunstler, K. Richter, R. Gerhard-Multhaupt, Ferroelectric polarization in stretched piezo-and pyroelectric poly (vinylidene fluoride-hexafluoropropylene) copolymer films, J. Appl. Phys. 92 (12) (2002) 7442–7447.

[12] R.G. Kepler, R.A. Anderson, Ferroelectric polymers, Adv. Phys. 41 (1) (1992) 1–57.

[13] L. Zhu, Q. Wang, Novel ferroelectric polymers for high energy density and low loss dielectrics, Macromolecules 45 (7) (2012) 2937–2954.

[14] S. Horiuchi, Y. Tokura, Organic ferroelectrics, Nat. Mater. 7 (5) (2008) 357–366.

[15] Y. Higashihata, J. Sako, T. Yagi, Piezoelectricity of vinylidene fluoride-trifluoroethylene copolymers, Ferroelectrics 32 (1) (1981) 85–92.

[16] D. Zhang, W. Liu, L. Tang, K. Zhou, H. Luo, High performance capacitors via aligned TiO$_2$ nanowire array, Appl. Phys. Lett. 110 (13) (2017), 133902.

[17] H. Luo, C. Ma, X. Zhou, S. Chen, D. Zhang, Interfacial design in dielectric nanocomposite using liquid-crystalline polymers, Macromolecules 50 (13) (2017) 5132–5137.

[18] Y. Wang, X. Zhou, Q. Chen, B. Chu, Q. Zhang, Recent development of high energy density polymers for dielectric capacitors, IEEE Trans. Dielectr. Electr. Insul. 17 (4) (2010) 1036–1042.

[19] L. Hang, D. Zhang, C. Jiang, X. Yuan, C. Chen, K. Zhou, Improved dielectric properties and energy storage density of poly (vinylidene fluoride-co-hexafluoropropylene) nanocomposite with hydantoin epoxy resin coated BaTiO$_3$, ACS Appl. Mater. Interfaces 7 (15) (2015) 8061–8069.

[20] J. Guiot, B. Ameduri, B. Boutevin, Radical homopolymerization of vinylidene fluoride initiated by tert- butyl peroxypivalate. Investigation of the microstructure by ^{19}F and ^{1}H NMR spectroscopies and mechanisms, Macromolecules 35 (23) (2002) 8694–8707.

[21] V.S.D. Voet, G. van Ekenstein, O.R. Gert, N.L. Meereboer, A.H. Hofman, G. ten Brinke, K. Loos, Double-crystalline PLLA-b-PVDF-b-PLLA triblock copolymers: preparation and crystallization, Polym. Chem. 5 (7) (2014) 2219–2230.

[22] I. Terzic, N.L. Meereboer, H.H. Mellema, K. Loos, Polymer-based multiferroic nanocomposites via directed block copolymer self-assembly, J. Mater. Chem. C 7 (4) (2019) 968–976.

[23] V.S.D. Voet, M. Tichelaar, S. Tanase, M.C. Mittelmeijer-Hazeleger, G. ten Brinke, K. Loos, Poly (vinylidene fluoride)/nickel nanocomposites from semicrystalline block copolymer precursors, Nanoscale 5 (1) (2013) 184–192.

[24] J.S. Wang, K. Matyjaszewski, Controlled/"living" radical polymerization. Atom transfer radical polymerization in the presence of transition-metal complexes, J. Am. Chem. Soc. 117 (20) (1995) 5614–5615.

[25] K. Matyjaszewski, J. Xia, Atom transfer radical polymerization, Chem. Rev. 101 (9) (2001) 2921–2990.

[26] K. Matyjaszewski, Atom transfer radical polymerization: from mechanisms to applications, Isr. J. Chem. 52 (3) (2012) 206–220.

[27] M. Kato, M. Kamigaito, M. Sawamoto, T. Higashimura, Polymerization of methyl methacrylate with the carbon tetrachloride/dichlorotris- (triphenylphosphine) ruthenium (II)/methylaluminum bis (2,6-di-tert-butylphenoxide) initiating system: possibility of living radical polymerization, Macromolecules 28 (5) (1995) 1721–1723.

[28] D.J. Keddie, A guide to the synthesis of block copolymers using reversible-addition fragmentation chain transfer (RAFT) polymerization, Chem. Soc. Rev. 43 (2) (2014) 496–505.

[29] G. Moad, E. Rizzardo, S.H. Thang, Living radical polymerization by the RAFT process, Aust. J. Chem. 58 (6) (2005) 379–410.

[30] J. Chiefari, Y.K. Chong, F. Ercole, J. Krstina, J. Jeffery, T.P.T. Le, R.T. A. Mayadunne, G.F. Meijs, C.L. Moad, G. Moad, Living free-radical polymerization by reversible addition-fragmentation chain transfer: the RAFT process, Macromolecules 31 (16) (1998) 5559–5562.

[31] L. Yang, E. Allahyarov, F. Guan, L. Zhu, Crystal orientation and temperature effects on double hysteresis loop behavior in a poly (vinylidene fluoride-co-trifluoroethylene-co-chlorotrifluoroethylene)-graft-polystyrene graft copolymer, Macromolecules 46 (24) (2013) 9698–9711.

[32] J. Wei, Z. Zhang, J.K. Tseng, I. Treufeld, X. Liu, M.H. Litt, L. Zhu, Achieving high dielectric constant and low loss property in a dipolar glass polymer containing strongly dipolar and small-sized sulfone groups, ACS Appl. Mater. Interfaces 7 (9) (2015) 5248–5257.

[33] L. Yang, J. Ho, E. Allahyarov, R. Mu, L. Zhu, Semicrystalline structure–dielectric property relationship and electrical conduction in a biaxially oriented poly (vinylidene fluoride) film under high electric fields and high temperatures, ACS Appl. Mater. Interfaces 7 (36) (2015) 19894–19905.

[34] Y.J. Yu, A.J.H. McGaughey, Energy barriers for dipole moment flipping in PVDF-related ferroelectric polymers, J. Chem. Phys. 144 (1) (2016), 014901.

[35] C. Cheng, E. Khoshdel, K.L. Wooley, Facile one-pot synthesis of brush polymers through tandem catalysis using Grubbs' catalyst for both ring-opening metathesis and atom transfer radical polymerizations, Nano Lett. 6 (8) (2006) 1741–1746.

[36] K. Matyjaszewski, N.V. Tsarevsky, Macromolecular engineering by atom transfer radical polymerization, J. Am. Chem. Soc. 136 (18) (2014) 6513–6533.

[37] T. Zhang, H. Nie, T.S. Bain, H. Lu, M. Cui, O.L. Snoeyenbos-West, A.E. Franks, K. P. Nevin, T.P. Russel, D.R. Lovley, Improved cathode materials for microbial electrosynthesis, Energy Environ. Sci. 6 (1) (2013) 217–224.

[38] D.A. Corbin, G.M. Miyake, Photoinduced organocatalyzed atom transfer radical polymerization (O-ATRP): precision polymer synthesis using organic photoredox catalysis, Chem. Rev. 122 (2) (2022) 1830–1874.

[39] X. Pan, C. Fang, M. Fantin, N. Malhotra, W.Y. So, L.A. Peteanu, A.A. Isse, A. Gennaro, P. Liu, K. Matyjaszewski, Mechanism of photoinduced metal-free atom transfer radical polymerization: experimental and computational studies, J. Am. Chem. Soc. 138 (7) (2016) 2411–2425.

[40] N.J. Treat, H. Sprafke, J.W. Kramer, P.G. Clark, B.E. Barton, J. Read de Alaniz, B. P. Fors, C.J. Hawker, Metal-free atom transfer radical polymerization, J. Am. Chem. Soc. 136 (45) (2014) 16096–16101.

[41] G. Yilmaz, Y. Yagci, Photoinduced metal-free atom transfer radical polymerizations: state-of- the-art, mechanistic aspects and applications, Polym. Chem. 9 (14) (2018) 1757–1762.

[42] X. Xu, X. Xu, Y. Zeng, F. Zhang, Oxygen-tolerant photoinduced metal-free atom transfer radical polymerization, J. Photochem. Photobiol. Chem. 411 (2021), 113191.

[43] N. Corrigan, J. Yeow, P. Judzewitsch, J. Xu, C. Boyer, Seeing the light: advancing materials chemistry through photopolymerization, Angew. Chem. Int. Ed. 58 (16) (2019) 5170–5189.

[44] I. Zaborniak, P.I. Chmielarz, K. Wolski, Riboflavin-induced metal-free ATRP of (meth) acrylates, Eur. Polym. J. 140 (2020), 110055.

[45] I. Zaborniak, P. Chmielarz, Riboflavin-mediated radical polymerization–Outlook for eco-friendly synthesis of functional materials, Eur. Polym. J. 142 (2021), 110152.

[46] Q. Ma, J. Song, X. Zhang, L. Ji, S. Liao, Metal-free atom transfer radical polymerization with ppm catalyst loading under sunlight, Nat. Commun. 12 (2021) 429.

[47] C.J. Mable, R.R. Gibson, S. Prevost, B.E. McKenzie, O.O. Mykhaylyk, S.P. Armes, Loading of silica nanoparticles in block copolymer vesicles during polymerization-induced self-assembly: encapsulation efficiency and thermally triggered release, J. Am. Chem. Soc. 137 (51) (2015) 16098–16108.

[48] S. Beyazit, S. Ambrosini, N. Marchyk, E. Palo, V. Kale, T. Soukka, B.T.S. Bui, K. Haupt, Versatile synthetic strategy for coating upconverting nanoparticles with polymer shells through localized photopolymerization by using the particles as internal light sources, Angew Chem. Int. Ed. Engl. 53 (34) (2014) 8919–8923.

[49] C. Kutahya, C. Schmitz, V. Strehmel, Y. Yagci, B. Strehmel, Near-infrared sensitized photoinduced atom-transfer radical polymerization (ATRP) with a copper (II) catalyst concentration in the ppm range, Angew Chem. Int. Ed. Engl. 57 (26) (2018) 7898–7902.

[50] T. Zhang, T. Chen, I. Amin, R. Jordan, ATRP with a light switch: photoinduced ATRP using a household fluorescent lamp, Polym. Chem. 5 (16) (2014) 4790–4796.

[51] C. Kutahya, F.S. Aykac, G. Yilmaz, Y. Yagci, LED and visible light-induced metal free ATRP using reducible dyes in the presence of amines, Polym. Chem. 7 (39) (2016) 6094–6098.

[52] X. Liu, L. Zhang, Z. Cheng, X. Zhu, Metal-free photoinduced electron transfer–atom transfer radical polymerization (PET– ATRP) via a visible light organic photocatalyst, Polym. Chem. 7 (3) (2016) 689–700.

[53] Z. Huang, Y. Gu, Z. Liu, L. Zhang, Z. Cheng, X. Zhu, Metal-free atom transfer radical polymerization of methyl methacrylate with ppm level of organic photocatalyst, Macromol. Rapid Commun. 38 (10) (2017) 1600461.

[54] S. Dadashi-Silab, X. Pan, K. Matyjaszewski, Phenyl benzo[b]phenothiazine as a visible light photoredox catalyst for metal-free atom transfer radical polymerization, Chem. Eur J. 23 (25) (2017) 5972–5977.

[55] G.M. Miyake, J.C. Theriot, Perylene as an organic photocatalyst for the radical polymerization of functionalized vinyl monomers through oxidative quenching with alkyl bromides and visible light, Macromolecules 47 (23) (2014) 8255–8261.

[56] A. Allushi, S. Jockusch, G. Yilmaz, Y. Yagci, Photoinitiated metal-free controlled/living radical polymerization using polynuclear aromatic hydrocarbons, Macromolecules 49 (20) (2016) 7785–7792.

[57] A. Allushi, C. Kutahya, C. Aydogan, J. Kreutzer, G. Yilmaz, Y. Yagci, Conventional Type II photoinitiators as activators for photoinduced metal-free atom transfer radical polymerization, Polym. Chem. 8 (12) (2017) 1972–1977.

[58] A. Isse, C.Y. Lin, M. Coote, A. Gennaro, Estimation of standard reduction potentials of halogen atoms and alkyl halides, J. Phys. Chem. B 115 (4) (2011) 678–684.

[59] A. Altomare, K. Loos, Metal-free atom transfer radical polymerization of PVDF-based block copolymers catalyzed by organic photoredox catalysts, Macromol. Chem. Phys. 224 (2023), 2200259.

[60] W. Tang, K. Matyjaszewski, Effects of initiator structure on activation rate constants in ATRP, Macromolecules 40 (6) (2007) 1858–1863.

[61] K. Xu, P. Khanchait, Q. Wang, Synthesis and Characterization of self-assembled sulfonated poly(styrene- b-vinylidenefluoride-b-styrene) triblock copolymers for proton conductive membranes, Chem. Mater. 19 (2007) 5937–5945.

[62] K. Li, S. Liang, Y. Lu, Q. Wang, Synthesis of telechelic fluoropolymers with well-defined functional end groups for cross-linked networks and nanocomposites, Macromolecules 40 (12) (2007) 4121–4123.

[63] R. Timmerman, W. Grayson, The predominant reaction of some fluorinated polymers to ionizing radiation, J. Appl. Polym. Sci. 6 (22) (1962) 456–460.